Process Modeling and Techno-Economic Analysis of a Solar Thermal Aided Low-rank Coal Drying-Pyrolysis Process

Tara Hosseini and Lian Zhang*

Department of Chemical Engineering, Monash University, Clayton, GPO Box 36, Victoria 3800, Australia

* Corresponding author: Email: lian.zhang@monash.edu

Tel: +61-3-9905-2592, Fax: +61-3-9905-5686

Abstract

This study investigated the feasibility of integration of concentrated solar power (CSP) to low-rank coal pyrolysis process from the economic and technical perspective. Upon a robust design of four different scenarios for the process integration, the effects of a variety of key variables have been examined, including different types of solar collectors, heat transfer fluids (HTF) and pyrolysis temperature. The plant operation analysis showed that integrating solar tower (ST) to provide heat for both coal drying and pyrolysis within the plant can save an average of 12.8% of the annual thermal energy demand. For the optimum solar tower design, it requires a solar multiple of 2, using carbonate salts as HTF, a design point D_{NI} of 750 W/m^2 and a heat storage capacity of 8 h to maximize its total solar energy output over a year. However, from an economical perspective, the use of solar tower for both drying and pyrolysis is economically infeasible. Instead, the parabolic trough solar collectors (PTC) designed to cover the heat required for coal drying only is most economically viable. It even shows a slightly better economic performance than the conventional pyrolysis process. The parabolic trough solar system assisted pyrolysis process has the potential to reach a high net present value (NPV) of $81.1 million and a short payback period of 4.9 years, relative to an NPV of $52.8 million and a payback period of 5.1 years for the conventional pyrolysis process.

Keywords

Low-rank coal, concentrated solar power, solar thermal-aided pyrolysis, techno-economic analysis.

1. Introduction

The utilization of renewable energies such as solar thermal energy is a promising way to reduce CO_2 emissions from the power generation and other energy-intensive industrial processes [1, 2]. In general, the concentrated solar power (CSP) technologies use the entire solar spectrum to provide a source of high-temperature process heat in the range of 500-2000°C that are employed to produce power, fuels and chemicals [3]. According to the International Energy Agency (IEA), fossil fuels continue to dominate heat supplies, while renewable energy met only 10% of the global industrial heat demand in 2018 [4]. A quick and easy transition from fossil fuel to renewable energies or bio-based energies is unlikely foreseeable in the near future. Instead, the hybridization of renewable energies with the existing fossil fuel reliant processes provides an economically viable option in the transition period [5].

In this paper, we aim to elaborate the feasility of integrating CSP into an existing proess for the pyrolysis of Victoria brown coal (VBC), the cheap and abundant resource in the state of Victoria, Australia [6]. Compared to combustion, pyrolysis bears a low CO_2 emission rate, and a high flexibility in the provision of multi-products including solid char, liquid fuel, and even syn-gas [7]. Apart from the two units including drying and pyrolysis, most of the downstream upgrading units are also highly endothermic, requiring a large energy input which is usually generated from the on-site combustion of a portion of the feedstock and/or products including char, liquid bio-oil or pyrolysis gas. This in turn reduces the producr yield and increases the unit emission amount of CO_2 [8, 9]. Alternatively, the integration of solar energy into the pyrolysis process is expected to overcome these problems [10]. In addition, it

assits in the storage of intermittent solar thermal energy in the form of transportable fuels derived from the pyrolysis process [11].

To date, the integration of solar system into pyrolysis has been researched, most of which are concerned for the high cost and intermittent solar radiation affected by cloud and rain [12]. From the technical perspective, researches have also been conducted to assess the use of solar concentrator to provide heat input to a receiver acting as a pyrolysis reactor for different biomass feedstocks [9, 13-23], coal [24], scrap rubber [25] and plastic wastes [26]. In these studies, the direct solar insolation is concentrated and redirected to the pyrolytic reactor by a solar concentrator mainly parabolic dishes or Fresnel lenses that only can attain medium and low temperatures in the pyrolysis reactors (up to 600°C) [27]. Hence, the temperature for pyrolysis highly depends on the availability of the sunlight [14, 28], the average temperature range of the solar concentrator, and even limited by contamination of the glass tube or window [29]. In addition, the intermittence of solar energy would result in an unstable product quality and yields that in turn affect the downstream units [30]. For instance, upon the use of a solar biomass pyrolysis system in a Linear Fresnel Reflector (LFR), the simulation results have confirmed a maximum char yield of 40.8 wt% on a typical metrological day in Seville, Spain. However, the annual average char yield only reaches 10.1 wt% in the case that the influence of irradiance level variation is taken into account [28]. Some studies have further considered the intermittent nature of the solar energy on a hourly basis, for the studies on power generation [31-33] or gasification [29, 34-36]. Zeaiter et al. took an integrated approach to simulate a waste tyre pyrolysis process integrated with CSP using linear Fresnel reflectors technology. They concluded that solar energy in Lebanon can provide on average 47.14% of the annual energy demands on the pyrolysis reactor [37]. However, the feasibility of this design from an economical point of view is a question.

To the best of our knowledge, there is still lack of study investigating the incorporation of CSP into a hybrid low-rank coal drying-pyrolysis process that utilizes a high temperature pyrolysis process in the range of 600-800°C. Compared to biomass, low-rank coal is much more abundant and stable across the world. It is thus significant to address how to use this resource in a low-emission manner in the future carbon-constrained world.

The focl point of this study is on the integration of CSP into the pyrolysis of VBC for the heat provision to two energy-intensive units, dryer and pyrolysis reactor. Two different pyrolysis temperatures of 600°C and 800°C, and two different CSP systems including parabolic trough collectors (PTC) and solar tower (ST) were considered. In addition, three different simulation tools have been coupled synergistically to eloaborate the optimum configuration of the CSP systems in terms of its integration with the pyrolysis process. Upon the design of different alternatives to the CSP system and sensitivity analyses, the most favorable design from economical and technical points of view was designed, which has the potential for a deployment in the future.

2. Modeling Approach

2.1 Simulation flowsheet

In this study, three different simulation platforms were integrated for the modeling, as shown in Figure 2**.** The simulation starts with the calculation of the hourly absolute efficiency of the solar receiver in MATLAB. The incident solar irradiation, receiver characteristics and geographic location were used as an input into MATLAB Daily performance modeling file,

generating three key outputs for the solar system, including absolute efficiency, available solar radiation and the daily radiation. Subsequently, these outputs were used as inputs into the System Advisor Model (SAM) software. Besides, to assist in specifying the details of the solar plant in SAM, the total energy required for the dryer and pyrolysis reactor were retrieved from the conventional pyrolysis process modeling in Aspen Plus. The key outputs determined from SAM include characteristics of the receiver and collector, and cost of the solar plant. In the next step, the annual solar energy available calculated by SAM was used as an input into the modified hybrid system. Aspen Plus flowsheet was used to finalize the specifications of the hybrid plant such as product yields, auxiliary power required and also cost of the process excluding the solar system. The details of each modeling approach are provided later.

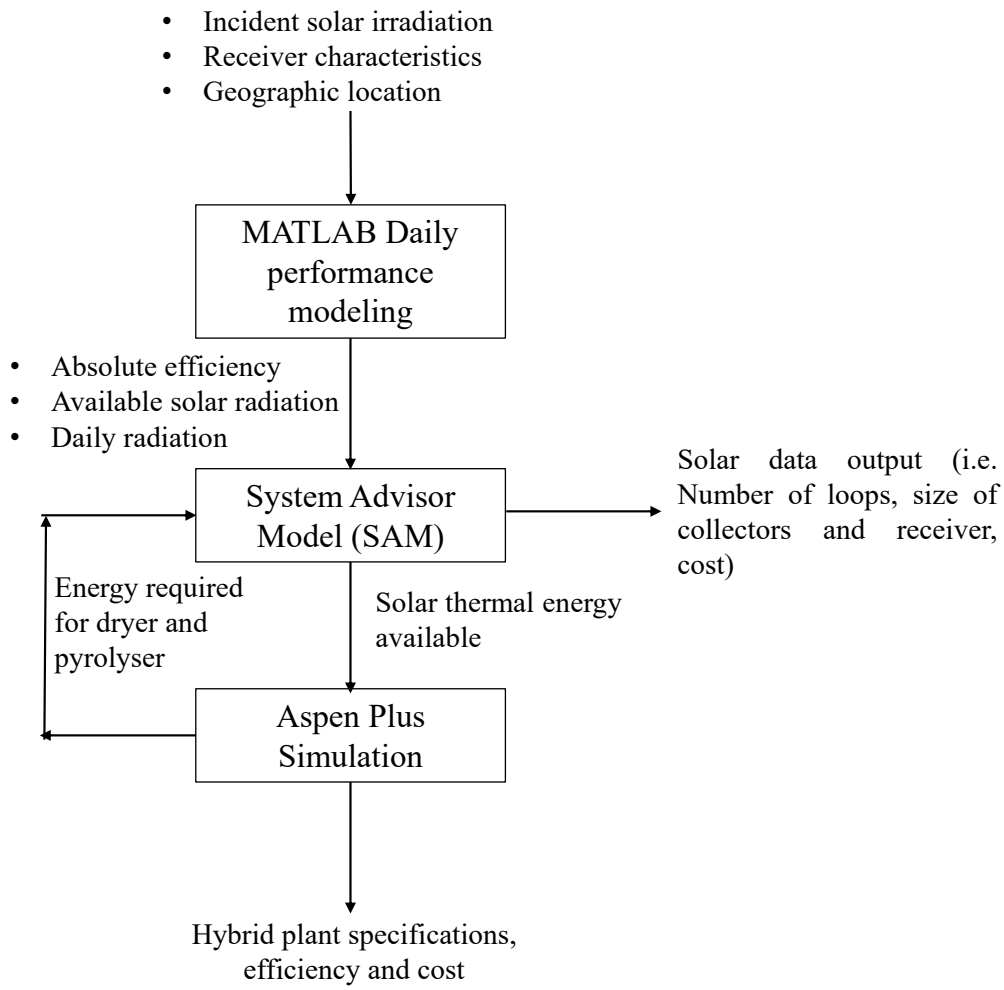

Figure 1 Simulation flowchart of the integrated pyrolysis process

2.2 VBC pyrolysis flowsheet in Aspen Plus

The VBC conventional pyrolysis process flowsheet built in Aspen Plus V 9.0 in our previous work [38] was used as an input. In brief, the virtual plant is designed to treat 70.6 t/h of wet VBC with an initial moisture content of 65 wt% through drying, briquetting, pyrolysis and downstream treatment in sequence. The energy required for the dryer and pyrolyser was supplied through burning a portion of syn-gas derived from the pyrolysis, dryer dust together with the loose particles remained from the briquetting process. Note that, the moisture content in coal is supposed to drop from 65% to 15% in an indirect rotary drum dryer with the coal outlet temperature of around 120°C. The pyrolysor in supposed to have two typical

temperatures, 600°C and 800°C. The former temperature is benefitical in maximising the liquid oil yield, whilst the latter one facilitates the syn-gas yield.

In a hybridized solar pyrolysis process, the concentrated solar energy acts as the main heating source to drive the pyrolysis process [39]. In addition to heating the pyrolyser which is the largest energy consumer in the process, solar energy is also utilized to dry the coal before passing through the pyrolysis reactor. The energy demands for the entire pyrolysis processes are listed in Table 1, which are extracted from the Aspen Plus simulation and used as a basis for the design of the CSP system. Note that, a back-up power is employed to run the pyrolysis process continuously when solar energy is not sufficient. The block-flow diagram of the hybrid process is depicted in Figure 2. The raw coal composition and the production yields of the conventional pyrolysis process at 800°C for the best-case scenario are presented in Table S1 [38] in the Supporting Information (SI). The details of the Aspen Plus model modification is also explained in the SI.

Table 1 Annual energy demand for the dryer and pyrolysis reactor

Equipment	Annual Thermal Energy required (MWh)	Annual Thermal Energy required (MWh/t raw coal)
Dryer	32.8	0.47
pyrolysis reactor (600°C)	13.9	0.2
pyrolysis reactor (800°C)	37.9	0.54

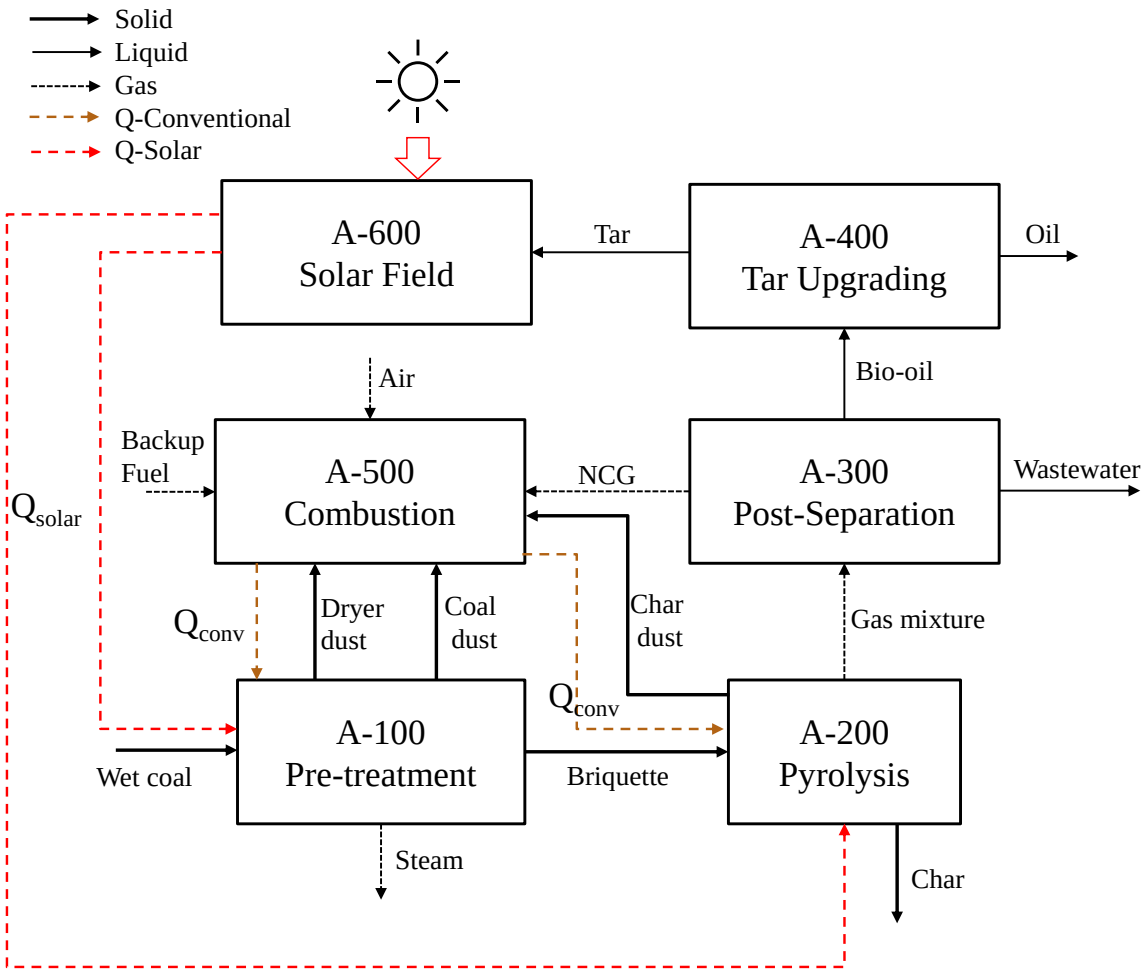

Figure 2 Block flow diagram of the integrated pyrolysis process

2.3 System Advisor Model (SAM) simulation

The SAM program developed by the National Renewable Energy Laboratory (NREL) was employed for the design of the solar thermal plant. In this study, SAM was used to simulate the solar thermal system over one entire year to accommodate the seasonal change on temperature. The change on temperature has a subsequent effect on the irradiated heat to be received by the CSP system and then its energy output. SAM calculates the solar field energy output on an hourly basis, which was subsequently summed across an entire year to determine the annual solar field energy output. It is used as a measure to compare the performance of each scenario.

2.3.1 Site Location

The Australian continent has the highest unit of solar radiation per square meter [40]. Solar energy resources are greater in the deserts in the northwest and central areas. However, harvesting solar energy in these two areas requires a high investment in transmission infrastructure [41]. For this research, Melbourne located in the southeast of Australia was selected as the reference site, considering that it houses abundant Victorian brown coal [42]. The weather file data for Melbourne is available in the SAM database, providing comprehensive hourly data for a whole year. The climatological data for this location is summarized in Table S2.

2.3.2 Solar Plant Design

2.3.2.1 Receiver and collector

Two common designs of the CSP solar systems are parabolic trough collectors (PTC) and solar tower (ST) [43]. The PTC is the most proven cost-effective technology using a heat transfer fluid (HTF) to collect heat energy from the sun [44]. The focal line temperature of the PTC receiver can be as high as 350-400°C [45], or even higher such as 550°C [46]. In this study, the Sky Fuel Sky Trough Collector Model with 80 mm OD receiver is selected for the design [47]. In contrast to the PTC system, an ST system can deliver a higher receiver temperature such as 500 – 1000°C [48] and a higher thermodynamic efficiency depending on the primary heat transfer fluid [49]. A higher operating temperature up to 1500°C has been reported in the literature [46]. An array of slightly concave mirrors called heliostats focuses the solar radiation onto an elevated central tower. To maximize the concentration ratio and to

191 decrease the solar energy loss, a secondary reflector is located at the top of the tower to re-
192 transmit radiation from the heliostat field to the receiver [50].

193 The solar tower can also be complemented with a thermal storage system (TES), which in
194 turn decrease the fluctuation of the operation of the entire process with the variation of the
195 solar radiation [2].

196

197 Considering the above-mentioned limits for the two different solar systems, four different
198 scenarios have been considered in this study, including:

199 1- Using PTC only as the heat source to integrate a direct steam generation (DSG)
200 system into the coal dryer, while burning a portion of pyrolysis gas to provide heat for
201 the pyrolysis reactor;
202 2- Using PTC only as the heat source to heat molten salt for the coal dryer, while
203 burning a portion of pyrolysis gas to maintain the pyrolyser;
204 3- Using ST as the heating source for both dryer and pyrolysis reactor at 600°C; and
205 4- Using ST as the heating source for both dryer and pyrolysis reactor at 800°C.

206

207 For the first two scenarios shown in Figure 3a, a PTC is used to heat the water/molten salt
208 through the reflection of the solar rays on the absorber tube/receiver. Afterwards, the hot
209 HTF, steam or molten salt is pumped to the coal dryer. HTF is finally circulated back to the
210 receiver once the drying duty is achieved. For the last two scenarios shown in panel b, a solar
211 tower system with two storage tanks is employed, consisting of a heliostat field, a receiver, a
212 storage system and a tower [2]. The biaxial tracked heliostats reflect the solar radiation onto
213 the central receiver installed on top of the solar tower. In this design, the HTF is pumped
214 from the cold storage tank to the evacuated receiver tubes which are heated up in the solar

system. The heated HTF then flows through both the dryer and the pyrolysis reactor. The finally cold molten salt is recirculated to the cold salt tank.

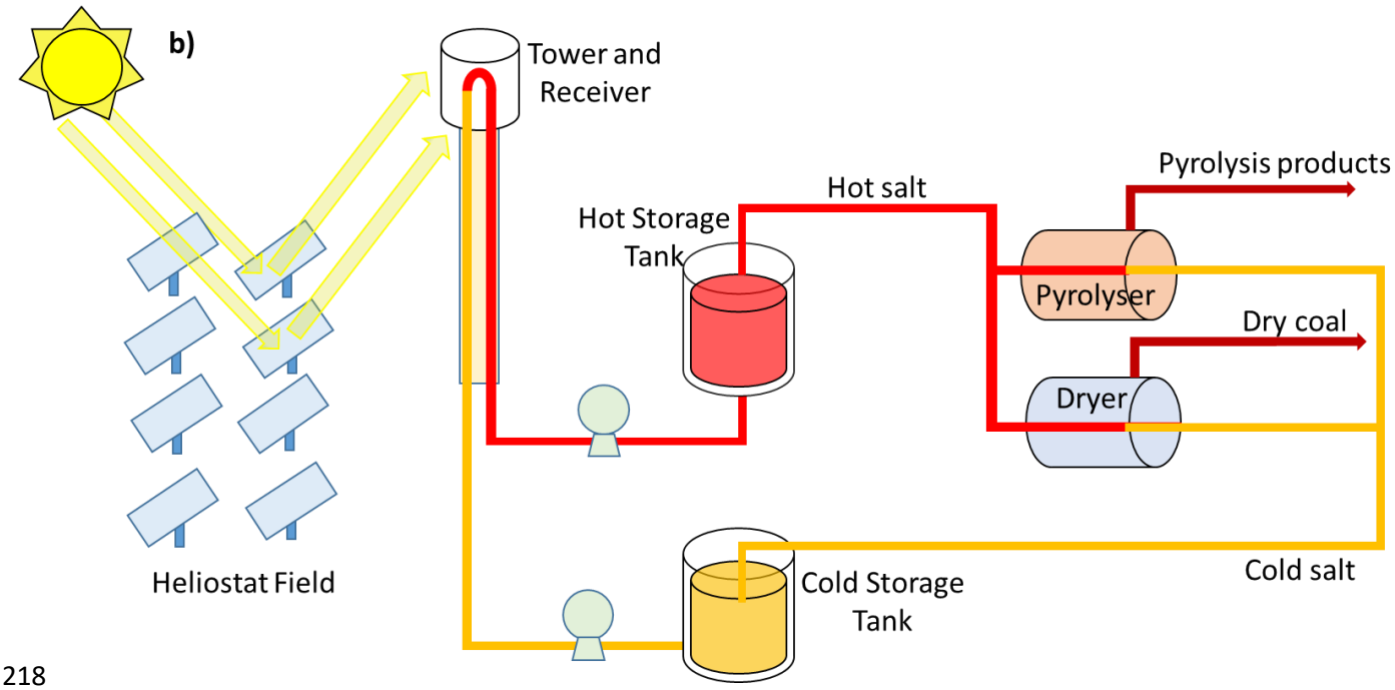

Figure 3 a) The Parabolic trough collector system utilized for acenarios 1 and 2 and b) Solar tower system used to design Scenario 3 and 4

2.3.2.2 HTF in the ST system

The heat transfer fluid is a key feature of the design as it requires unique properties such as high thermal storage density [37], an excellent heat transfer rate and long-term durability [45]. Water/steam is ideal when power generation is the design purpose, whilst liquid sodium, oil or molten salts is preferened when heat storage is required [50]. Out of the different types of liquid and solid-state heat storage materials, molten salts are the ideal materials in a solar power plant [51]. Among the different types of molten salts, carbonate salts show wide working temperature (450-850°C) [45, 48], which are thus selected in this study. Table 2 presents the assumptions and specifications used in the SAM system for the four scenarios. The design point represents the direct normal irradiance available at the plant location. The direct irradiance received on a plane normal to the sun is called direct normal irradiance (D_{NI}) [52]. SAM uses a default value of 950 W/m^2 which corresponds to the sun position at noon on the summer solstice. The target solar multiple is a design ratio of heat sink power to the target receiver thermal power which is the amount of thermal energy received at the receiver outlet [53]. For scenarios 1 and 2, since there is not any potential for energy storage, the solar multiple of 1 was selected; while for scenarios 3 and 4, the solar multiple was set at the default value of 1.4 in the SAM. The target receiver thermal power values entered to the model are adopted from Table 1, according to the solar thermal requirement of each scenario. Loop inlet and outlet HTF temperatures refer to the inlet and outlet temperature of the HTF entering and exiting the loop at the design point. Pressurized water and Hitec solar salt were selected as HTF for scenarios 1 and 2 respectively and the operating temperature range of the HTF was adopted from the SAM. For scenarios 3 and 4, the HTF inlet and outlet temperature were chosen from the operating temperature range (from the melting temperature to the boiling temperature) of the carbonate salt [48].

Table 2 The assumptions and justifications used to design the four scenarios

	Scenario 1	Scenario 2	Scenario 3	Scenario 4
Design point D_{NI} (kW/m^2)	950	950	950	950
Target solar multiple	1	1	1.4	1.4
Heat sink power (MW)	32.8	32.8		
Target receiver thermal power (MW)	32.8	32.8	46.7	70.7
Energy Storage (h)	No	No	1 h	
HTF	Pressurized water	Hitec Solar Salt ($NaNO_3$-$NaNO_2$-KNO_3)	Carbonate Salts (Li_2CO_3-Na_2CO_3-K_2CO_3)	
Loop inlet HTF temperature (°C)	120	238	550	
Loop outlet HTF temperature (°C)	180	529	821	

2.4 Daily Performance Modeling

The daily performance of the plant as the starting point in Figure 1 was modelled in MATLAB to calculate the absolute efficiency ($\eta_{absolute}$). The absolute efficiency is a measure to indicate the overall efficiency of a CSP system by taking into account several factors such as mirror cleanliness, reflectivity, shadow effects and incident angle. The detailed calculation procedure is explained in the SI.

2.5 Cost calculation methodology

Cost can be calculated by different measures, and each way of accounting for the cost of CSP bring its own insights [54] The analysis of cost can be very detailed but for comparison purposes, the approach used here is a simplified one. Although every effort has been made to give a realistic price, the rapid growth of renewable energy market, makes analysing the cost of CSP technologies challenging [54]. In this study, Levelized cost of Energy (LCOE) and Net Present Value (NPV) analysis have been used as cost indicators. LCOE that can be used

as an economic measure for both CSP and photovoltaic system (PV) is calculated by equation 1 shown below:

$$LCOE = \frac{FCR \times CC + FOC}{Annual\ energy} \quad (1)$$

Where FCR refers to a fixed charge rate, CC for capital cost and FOC for the fixed operating cost. The solar field annual thermal energy output is derived from SAM in MWh and the LCOE is reported in A$/MWh. The cost of energy production from the solar field per unit of thermal energy can be compared with other sources of energy. LCOE allows us to compare the different technologies of unequal life spans, project size, capital cost, risk, return, and capacities [55].

In addition to the LCOE as a measure to compare the different scenarios, Aspen Process Economic Analyzer and a cost estimation methodology developed by the Commonwealth Scientific and Industrial Research Organization (CSIRO) [56] were used to evaluate the capital cost and operating cost of the pyrolysis process excluding the solar system. The detailed assumptions and methodology for the cost calculation are explained in our previously published papers [38, 57]. The operating cost and capital cost of the solar system were derived from the SAM software. Operating cost of the pyrolysis plant was calculated as the summation of raw materials, utilities, total fixed charges, depreciation and capital.

3. Results and discussions

3.1 Daily performance modeling results

The 3-D results of the MATLAB modeling for a typical solar filed on a daily basis is presented in Figure 4. Panel *a* shows the D_{NI} values derived from the NREL weather file data and Panel *b* shows the D_{II} values after applying the efficiency factors on D_{NI}. As expected, there is an increase in both D_{NI} and D_{II} from morning to the noon at around 12-1 pm and then decline in the beam irradiance from noon to the sunset for each day. However, there is a broad variation from day to day, as demonstrated by a sharp decline of both D_{II} and D_{NI} from the start of the year (January) to the middle of the year (June), and then increase again until the end of the year (December).

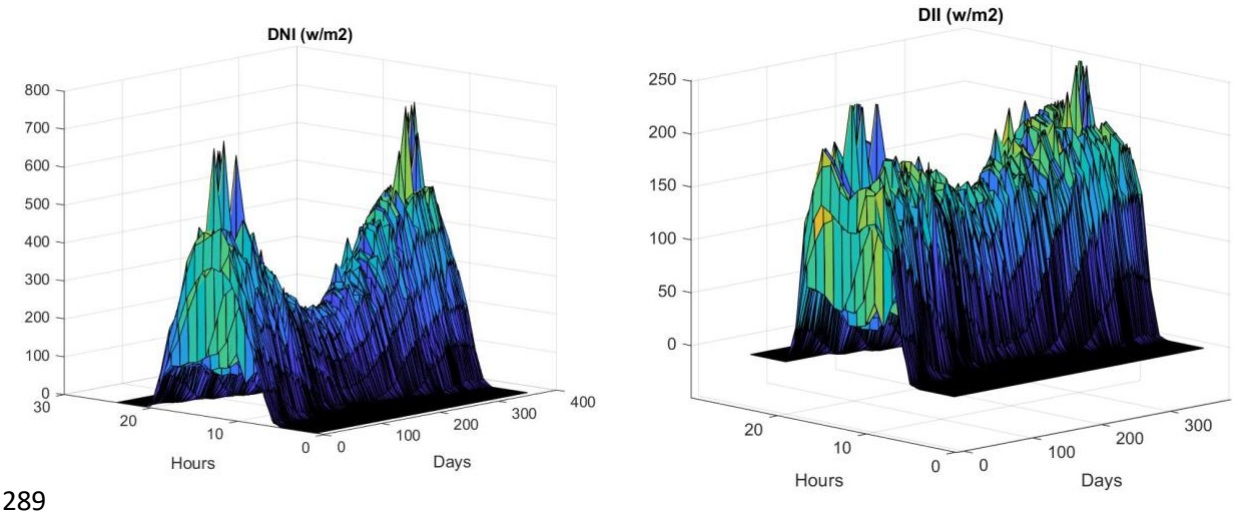

Figure 4 Daily performance modeling of a typical solar plant in Melbourne for 365 days and 24 hours of the day a) D_{NI} and b) D_{II}

The maximum irradiance for the D_{NI} and D_{II} values are 729 W/m^2 and 266 W/m^2, respectively, while the maximum value is only 0.72 for the absolute efficiency calculated by the MATLAB file. The reason for the slight difference in the D_{II} and D_{NI} trends is related to the strong effect of absolute efficiency which is low from 9 am to 4 pm.

3.2 SAM simulation results

3.2.1 System design output

Table 3 summarizes the system design output for the four design scenarios based on the SAM software. The PTC design for both scenarios 1 and 2 requires a loop number of 19, and a total aperture reflective area of 49,856 m^2 for both solar fields used for the coal drying only. This number was calculated based on the aperture reflective area of a single collector multiplied by the number of loops. The actual solar multiple of 1.01 found here is also close to the default value of 1 in the software system. A loop optical efficiency of 0.72 was found for both scenarios. This value was determined by the efficiency of collectors and receivers, whereas the thermal loss from the piping and the receivers was ignored here. The length of a collector single module for both scenarios was calculated to be around 14.4 m that are a standard size for Sky Fuel Sky Trough collectors [47].

Table 3 The design output from SAM for four different scenarios

	Scenario 1	Scenario 2		Scenario 3	Scenario 4
Type of system	PTC	PTC	Type of system	ST	ST
Actual number of loops	19	19	Receiver height (m)	6.71	7.75
total aperture reflective area (m^2)	49,856	49,856	Receiver diameter (m)	5.8	7.3
Actual solar multiple	1.01	1.01	Tower height (m)	68.3	81
Loop optical efficiency	0.7218	0.7218	Heliostat count	846	1272
Length of a collector single module (m)	14.375	14.375	Single heliostat area (m^2)	144.4	144.4
			Storage tank volume (m^3)	232	331

Regarding scenarios 3 and 4, using ST as the energy concentrator, their optimized receiver and heliostat layouts are presented in Figure 5 to supplement the dimension data in Table 3. As can be seen from both Table 3 and Figure 5, the receiver at the top of the tower is located in the center of a circle and the heliostats which are square mirrors with a surface area of 144.4 m^2, are dispersed on concentric circles. The solar field in scenario 4 is larger in the dimensions, due to the larger energy requirement for the high-temperature pyrolysis reactor. Compared to the receiver with a dimension of 6.71 m high and 5.8 m of diameter in scenario 3, the receiver in scenario 4 reaches 7.75 m high and 7.3 m of the diameter. The tower is also

much taller in scenario 4, reaching 81 m in comparison to 68.3 m for scenario 3. The number of heliostats accounts for 846 in scenario 3, which is smaller than scenario 4 requiring 1272. In terms of the HTF storage tank volume, it is around 232 m^3 for scenario 3, relative to 331 m^3 for scenario 4 to accommodate the excess energy requirement.

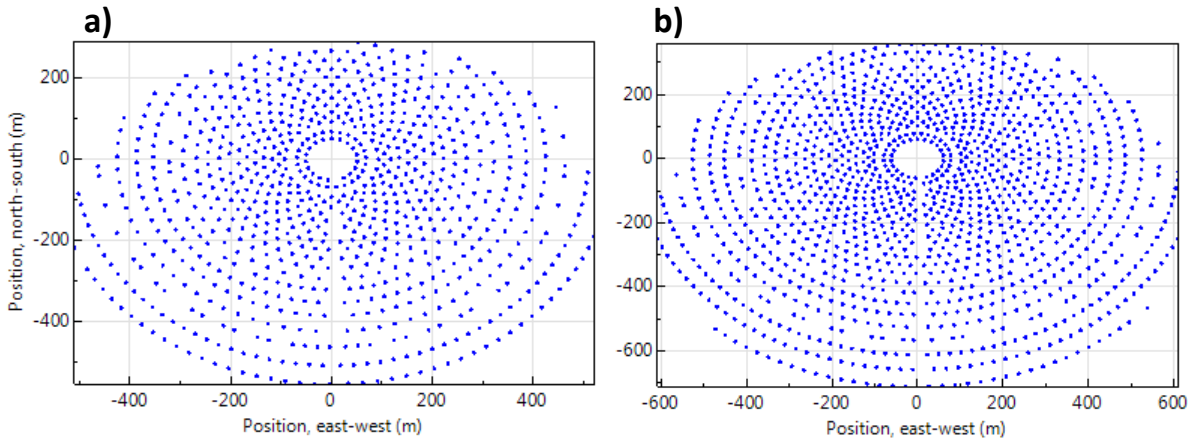

Figure 5 Optmized heliostat layout for a) Scenario 3 and b) Scenario 4

3.2.2 Solar field thermal energy output and input to the Aspen Plus

The solar field thermal energy output from the SAM simulation results was used as an input into the Aspen Plus model. This value is required to calculate the product yields and the backup power required. The process flowsheet for the four scenarios designed in Aspen Plus is shown in **Error! Reference source not found.**. To achieve the desired inlet and outlet HTF temperatures, the HTF flow rate was adjusted and backup power was added to the system once the solar thermal energy did not meet the target energy.

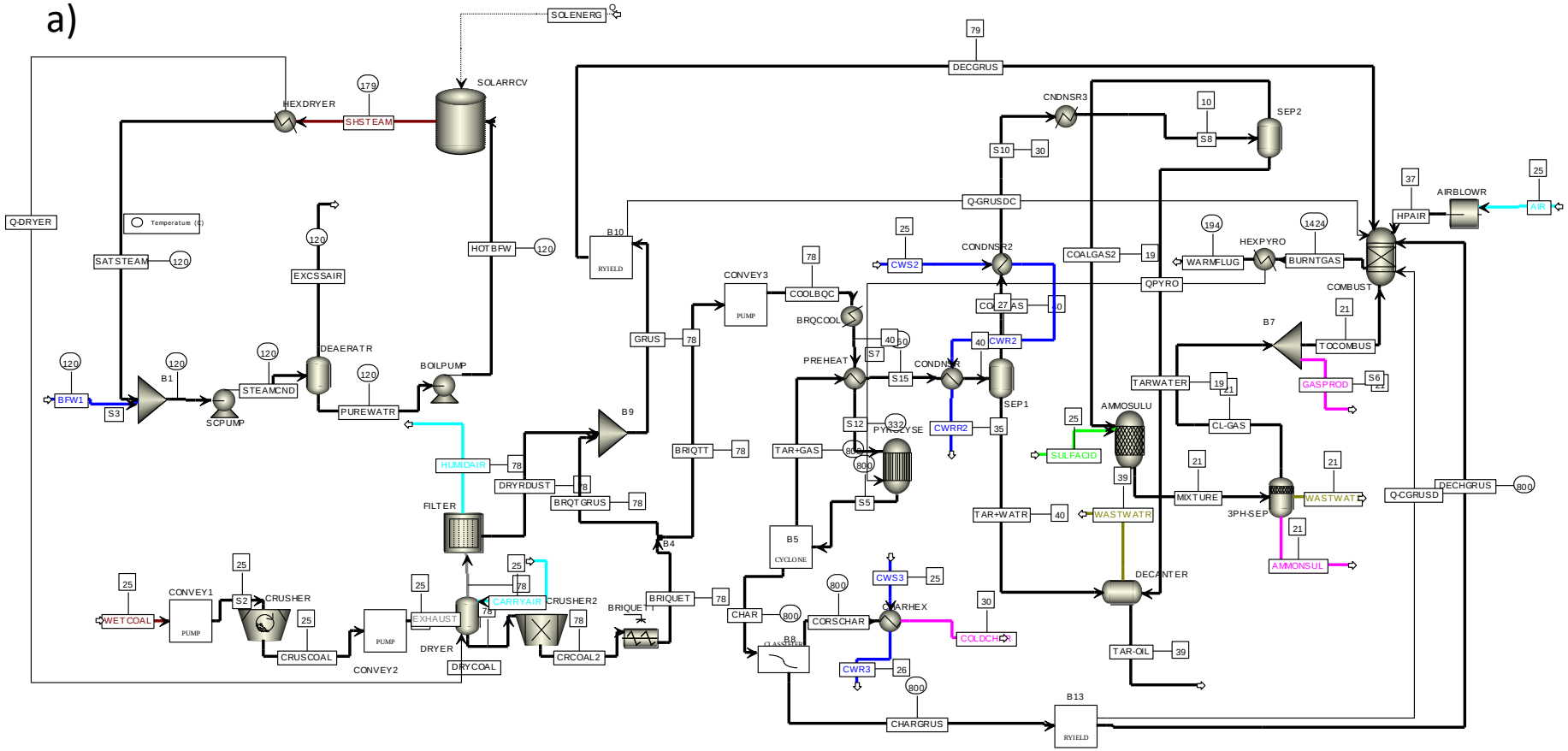
a)
SOLENERG
SOLARRCV
HEXDRYER
SHSTEAM
Q-DRYER
Temperature (C)
SATSTEAM
EXCSSAIR
HOTBFW
DEAERATR
BOILPUMP
BFW1
B1
S3
SCPUMP
STEAMCND
PUREWATR
HUMIDAIR
FILTER
DRYRDUST
BRQTGRUS
B9
B10
RYIELD
GRUS
CONVEY3
PUMP
COOLBQC
BRQCOOL
PREHEAT
S7
S15
S12
PYROLYSE
TAR+GAS
BRIQTT
B4
B5
CYCLONE
CHAR
CORSCHAR
CWS3
CHARHEX
COLDCHAR
CWR3
CHARGRUS
B13
B8
CONVEY1
CRUSHER
S2
WETCOAL
CRUSCOAL
CONVEY2
EXHAUST
DRYER
DRYCOAL
CARRYAIR
CRUSHER2
CRCOAL2
BRIQUET
BRIQUETT
DECGRUS
CNDNSR3
SEP2
S8
S10
Q-GRUSDC
CWS2
CONDNSR2
CWR2
SEP1
CONDNSR
CWRR2
COALGAS2
QPYRO
WARMFLUG
HEXPYRO
BURNTGAS
HPAIR
AIRBLOWR
AIR
COMBUST
B7
TOCOMBUS
GASPROD
TARWATER
CL-GAS
AMMOSULU
SULFACID
TAR+WATR
WASTWATR
DECANTER
TAR-OIL
MIXTURE
3PH-SEP
WASTWAT
AMMONSUL
Q-CGRUSD
DECHGRUS

b)

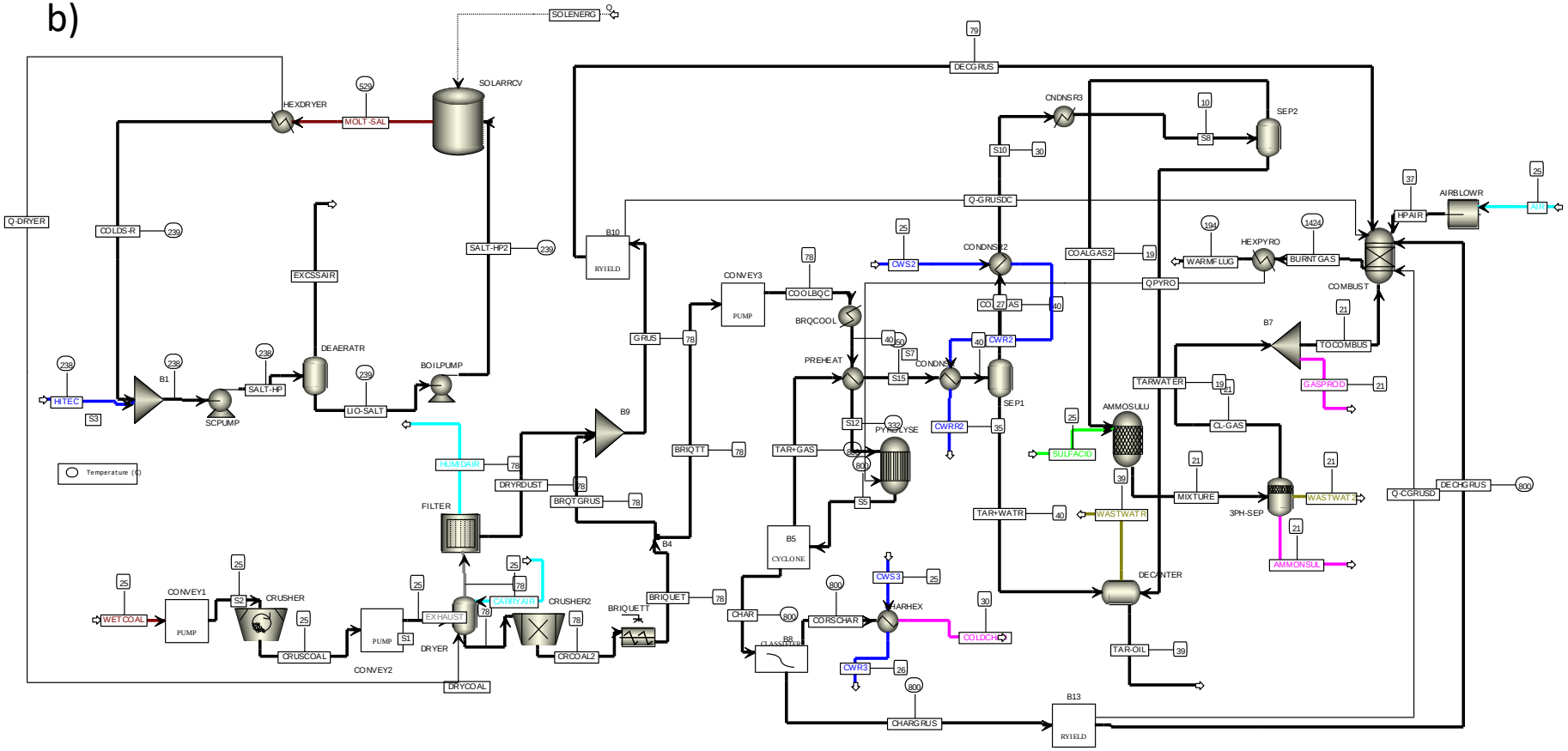
SOLENERG
SOLARRCV
HEXDRYER
MOLT-SAL
Q-DRYER
COLDS-R
SALT-HP2
EXCSSAIR
DEAERATR
BOILPUMP
HITEC
B1
SCPUMP
SALT-HP
LIO-SALT
S3
Temperature (C)
HUMDAIR
FILTER
DRYRDUST
BRQTGRUS
B9
B10
RYIELD
GRUS
CONVEY3
PUMP
COOLBQC
BRQCOOL
PREHEAT
BRIQTT
TAR+GAS
PYROLYSE
CONDNS1
CONDNSR2
CWS2
CWR2
SEP1
S15
S12
S7
S5
B5
CYCLONE
B4
BRIQUET
BRIQUETT
CHAR
CORSCHAR
MARHEX
CWS3
COLDCH
CWR3
B8
CLASSIFIER
CHARGRUS
B13
DECGRUS
CNDNSR3
SEP2
S10
S8
Q-GRUSDC
COALGAS2
WARMFLUG
HEXPYRO
BURNTGAS
QPYRO
COMBUST
HPAIR
AIRBLOWR
AIR
B7
TOCOMBUS
GASPROD
TARWATER
CL-GAS
AMMOSULU
SULFACID
TAR+WATR
WASTWATR
DECANTER
TAR-OIL
MIXTURE
3PH-SEP
WASTWAT2
AMMONSUL
Q-CGRUSD
DECHGRUS
WETCOAL
CONVEY1
CRUSHER
CRUSCOAL
CONVEY2
DRYER
EXHAUST
CARRYAIR
CRUSHER2
CRCOAL2
DRYCOAL

c)

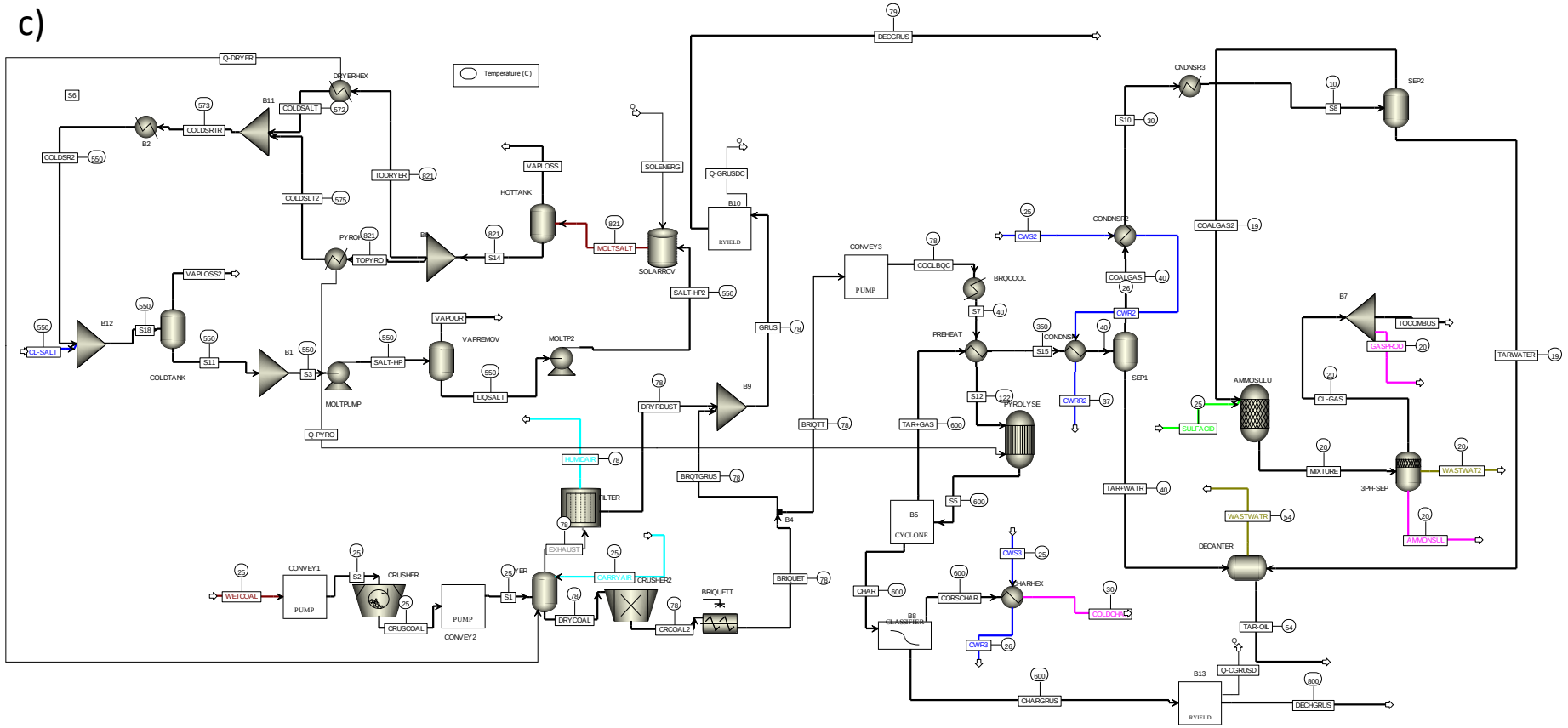
Q-DRYER
DRYERHEX
Temperature (C)
S6
B11
COLDSALT
572
573
B2
COLDSRTR
COLDSR2
550
TODRYER
821
COLDSLT2
575
PYRO
TOPYRO
B6
S14
VAPLOSS
HOTTANK
SOLENERG
Q-GRUSDC
B10
RYIELD
MOLTSALT
SOLARRCV
SALT-HP2
DECGRUS
79
CNDNSR3
SEP2
S10
30
10
S8
CONVEY3
PUMP
COOLBQC
78
BRQCOOL
S7
40
CONDNSR2
CWS2
25
COALGAS
26
COALGAS2
19
CWR2
B7
TOCOMBUS
GASPROD
20
TARWATER
19
PREHEAT
CONDNSR
S15
350
40
SEP1
S12
122
PYROLYSE
CWRR2
37
AMMOSULU
SULFACID
CL-GAS
MIXTURE
3PH-SEP
WASTWAT2
AMMONSUL
TAR+WATR
WASTWATR
54
DECANTER
TAR-OIL
S4
Q-CGRUSD
B13
RYIELD
DECHGRUS
800
CHARGRUS
600
VAPLOSS2
B12
S18
CL-SALT
COLDTANK
S11
B1
S3
MOLTPUMP
SALT-HP
VAPOUR
VAPREMOV
LIQSALT
MOLTP2
Q-PYRO
GRUS
BRQTT
TAR+GAS
600
B9
DRYRDUST
BRQTGRUS
HUMDAIR
FILTER
EXHAUST
B4
B5
CYCLONE
S5
CHAR
CORSCHAR
CHARHEX
CWS3
COLDCHAR
B8
CLASSIFIER
CWR3
26
WETCOAL
CONVEY1
PUMP
S2
CRUSHER
CRUSCOAL
PUMP
CONVEY2
S1
DRYER
DRYCOAL
CARRYAIR
CRUSHER2
CRCOAL2
BRIQUETT
BRIQUET

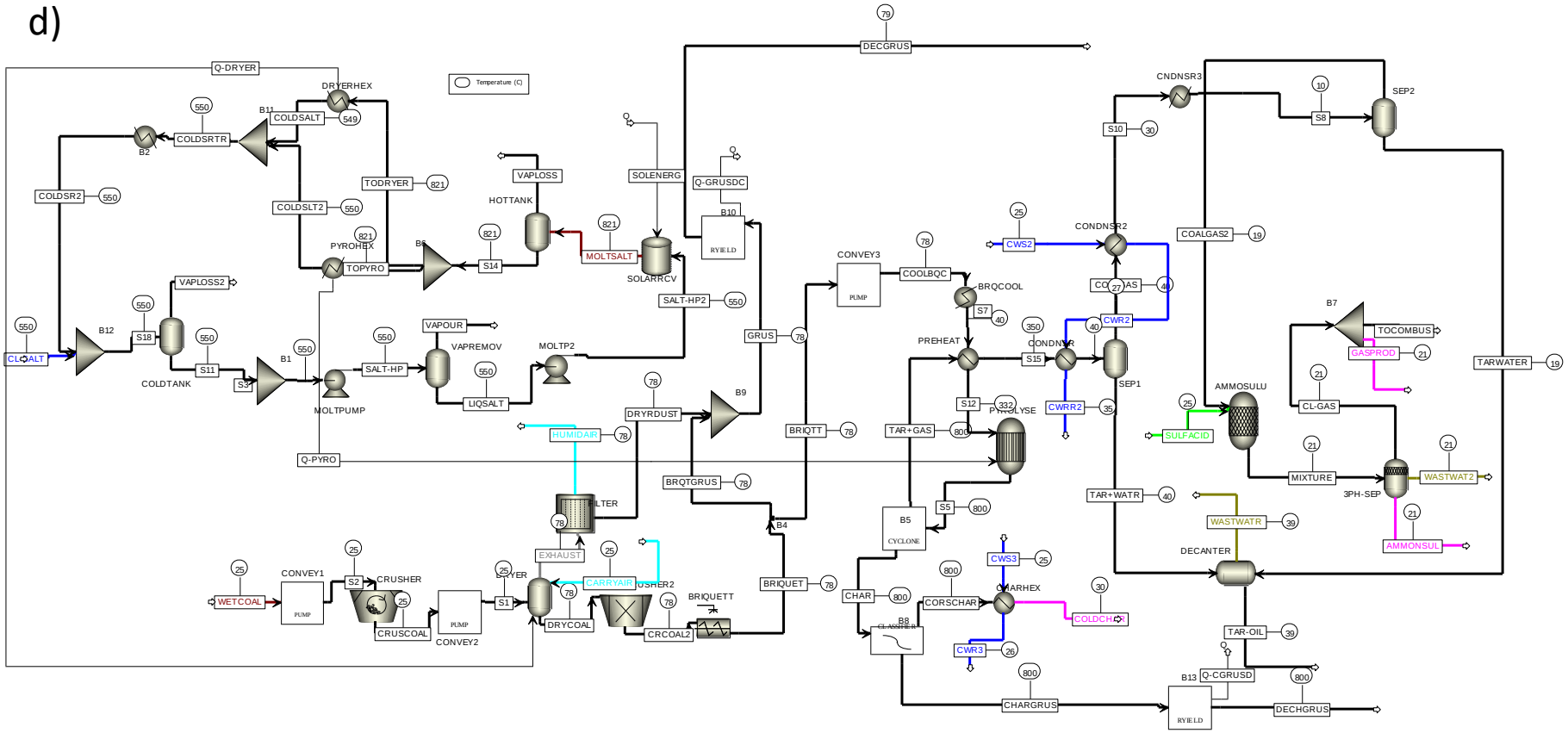

Figure 6 The integration of the CSP into Aspen Plus design for a) Scenario 1-using DSG for dryer only b) scenario 2-using molten salt for dryer only, c) scenario 3-using molten salt for both dryer and pyrolysis at 600°C and d) scenario 4-using molten salt for dryer and pyrolyser at 800°C

In scenario 1, boiler feed water with a temperature of 120°C and pressure of 0.3 MPa is pumped to the solar receiver. It was further heated to 180°C and pressurized to 0.4MPa upon receiving the solar heat. From the simulation and based on the target energy required, the maximum inlet flow rate of the boiler feedwater is 13.75 kg/s. This happens when the solar energy output is enough to heat the dryer to the desired temperature. In the direct steam generation unit, the steam produced is pumped directly to the dryer. Since no solar heat is provided for the pyrolyser, approximately 28% of the pyrolysis gas product (mainly CO, CH_4 and H_2) has to be consumed by the pyrolysis reactor. Therefore, the net gas product yield for this scenario is only 7.2 t/h. However, this value is higher than the reference case with a gas yield of only 4.11 t/h [38] due to the consumption of pyrolysis gas for both coal dryer and pyrolysis reactor in the reference case. Scenario 2 is almost the same as scenario 1 in terms of energy supply for the pyrolysis reactor. The only exception is that the maximum flow rate of the HTF entering the loop has to reach 59.5 kg/supply, due to providing energy for the dryer. This is almost four times larger than steam. Scenario 3 models a pyrolysis process at a low operating temperature of 600°C. Since the pyrolysis process is sensitive to the temperature, the amount and the composition of the pyrolysis gas is changed [58]. Although no pyrolysis gas is required to supply the heat for the pyrolysis reactor, the amount of pyrolysis gas left as a product is only 6.9 t/h, compared to the scenario 1 and 2 where a higher temperature of 800ºC is employed to devolatilize more coal into liquid products [58]. The maximum inlet flow rate of HTF was increased to 92 kg/s for scenario 3, and further to 126.5 kg/s for scenario 4, due to the provision of energy to both dryer and coal pyrolyser which is more than scenario 1 and 2. As a return, the yield of gas product is maximized in scenario 4 because no pyrolysis gas is consumed and the high pyrolysis temperature favors coal devolatilization.

The summary of the design parameters achieved from Aspen Plus together with the total thermal energy required (from Aspen Plus) and the annual solar field thermal energy output (from SAM) for all of the four scenarios are presented in Table 4. The percentage of solar thermal contribution for each scenario was calculated by dividing the annual solar field thermal energy output by the total thermal energy required. The resultant numbers are also included in Table 4. The annual solar field thermal energy output for scenario 4 is the largest among the four scenarios. For this scenario, around 12.82% of the total thermal energy required needs to be supplied from the designed solar system. Scenario 3 is the second largest for an annual solar field thermal energy output with 51.3 GWh to replace the thermal energy. The designed system for scenario 3 can contribute to 12.5% of the total thermal energy required. Scenario 1 is the third largest solar thermal supplier with 33.2 GWh of thermal energy, demonstrating the preference of steam over molten salt (scenario 2) for the drying unit. The system designed under scenario 1 can replace 11.56% of the total thermal energy required for a whole year, while scenario 2 with molten salt can only substitute 9.96% of the total thermal energy required. The monthly breakdown of the solar power supply for each scenario is further demonstrated in Figure 7. Regardless of the design scenario, there is a drastic change in the solar thermal power output upon the variation of the season. In the warmest and coldest months of a year, approximately 7 MW and 0.5 MW of solar power can be harvested respectively for scenario 1, which is equivalent to 21.3% and 1.6% of the total power required for the overall process. For scenario 2, the contribution of the warmest month reaches 6.3 MW, which drops significantly to only 0.2 MW of solar power in the coldest weather. DSG enables the implementation of a high steam temperature with a capacity to use the latent heat of the steam. This leads to a better cycle efficiency compared to molten salt [59, 60]. Scenarios 4 shows the best performance with 15.5 MW for January and 1.6 MW for

June which is slightly higher than scenario 3 with 10 MW and 1.0 MW for January and June, respectively.

Table 4 Solar system performance for the four designed scenarios derived from Aspen Plus and SAM

	scenario 1	scenario 2	scenario 3	scenario 4
HTF maximum Flow rate (kg/s)	13.75	59.5	92	126.5
Extra coal gas required for the pyrolysis reactor	28%	28%	No	No
Amount of coal gas left as a product (t/h)	7.2	7.2	6.9	10
The total thermal energy required (GWh)	287	287	410	620
Annual solar field thermal energy output (GWh)	33.2	28.6	51.3	79.4
Percentage of solar thermal contribution (%)	11.56	9.96	12.53	12.82

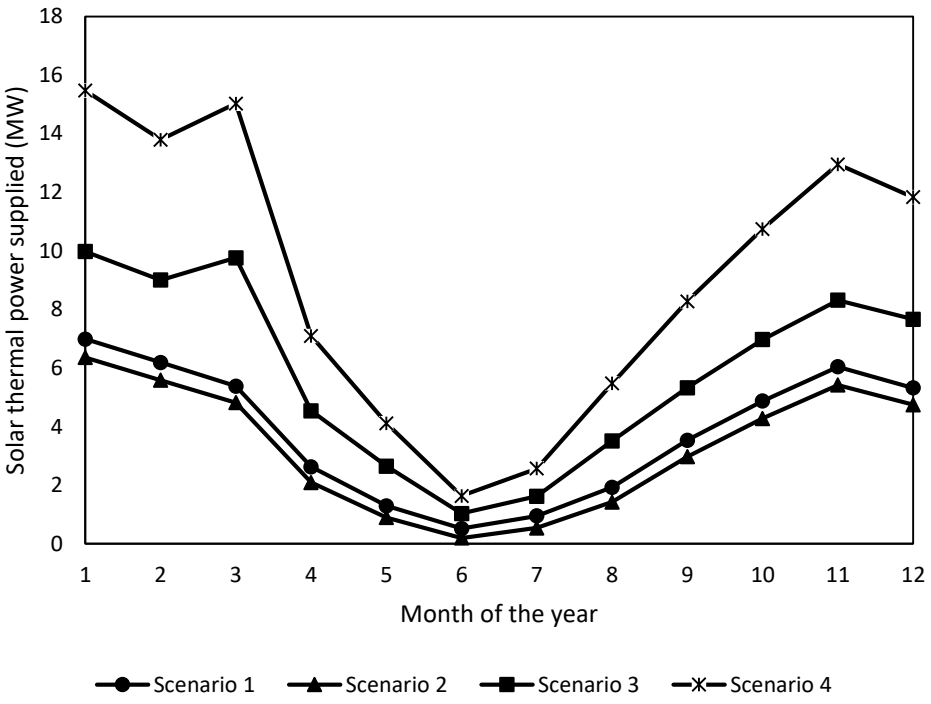

Figure 7 The average monthly break-down of the solar thermal power production for the four designed scenarios

3.3 Solar Field Cost Analysis

Figure 8 depicts the LCOE produced by the solar field through four designed scenarios, as compared with the other sources of energy production in Australian Dollar per Mega Watts hour of thermal energy (A$/MWh).

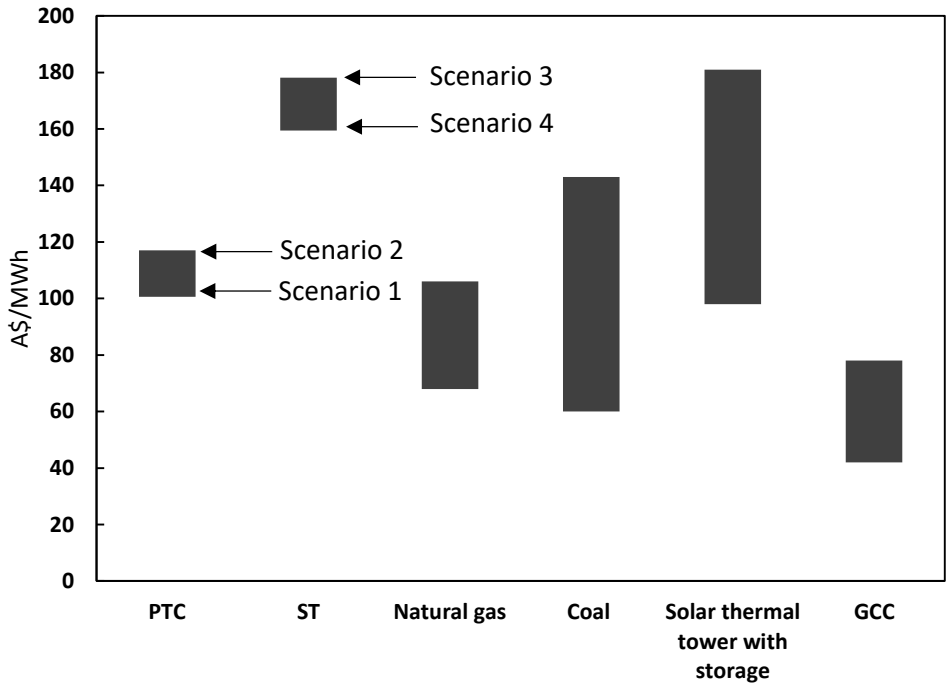

Figure 8 Comparison of the levelized cost of energy (LCOE) for four designed scenarios with other sources of energy (GCC: Gas combined cycle, PTC: Parabolic Trough collector and ST: Solar tower)

The LCOE of the solar field for Scenario 1 is the least with an LCOE of only A$101/MWh. Scenario 2 is slightly higher than scenario 1, reaching A$117 per MWh of the power produced. Scenario 3 is the most expensive scenario with A$178.1/MWh whilst scenario 4 exhibits a slightly lower LCOE of A$159.5/MWh. The LCOE of the two types of solar receivers investigated in this study is also comparable with that has been reported elsewhere [61]. Scenario 1 and 2 comprising PTC is located at the lower end of the LCOE bar chart of the reference ST with a price range of A$98-181/MWh [61]. However, the other two scenarios of 3 and 4 utilizing ST are located at the high end of the bar chart, demonstrating a high cost for these two CSP systems. The LCOE for all the four scenarios is also larger than the other energy systems including a gas combined cycle (GCC) of around A$42-78/MWh only, a coal-based power plant of $60 to 143/MWh, and a natural gas power plant varying between A$68 and $106/MWh.

3.4 Sensitivity Analyses

The sensitivity analysis was performed to find the optimum design conditions for scenario 4 considering that it is the most comprehensive option and the most probable design to be implemented in the industry. The parameters assessed include solar multiple, design value input D_{NI} and the thermal energy storage time.

3.4.1 Effect of design point D_{NI}

The change of design point D_{NI} is expected to alter the total solar thermal energy produced by the solar field. The effect of a change in the design point D_{NI} on the solar energy amount of scenario 4 and its LCOE is presented in Figure 9. With decreasing the design point D_{NI} from 950 to 750 W/m^2, the total solar field thermal energy output is increased from 79.4 to 99.7 GWh. In the meanwhile, the LCOE is decreased from A$159.5/MWh to A$133.5/MWh. Although the capital cost is increased with the addition of more heliostats and a larger field area to accommodate a larger solar energy production, the LCOE is decreased. The main reason is because of the production of more solar thermal energy from the system with a lower design point D_{NI} of 750 W/m^2. Since the annual average irradiation in Melbourne is around 750 W/m^2 over the year, the decrease in the design point D_{NI} to 750 W/m^2 is beneficial for the local solar field design.

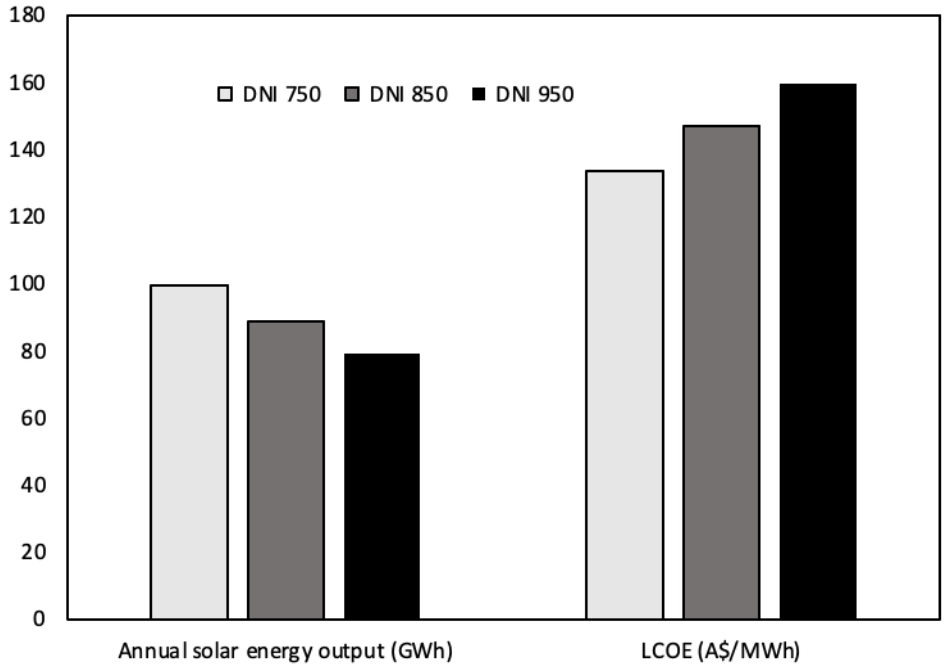

Figure 9 The effect of a change in the design point DNI on the annual solar thermal energy output and also LCOE for scenario 4

3.4.2 Effect of Solar Multiple

The SAM software sets a default value of 1.4 as the solar multiple for a solar thermal tower. Increasing the solar multiple results in a solar field that causes an increase in the solar field aperture area and header pipe length. Hence, a larger HTF temperature can be achieved [47]. This, in turn, results in an increased workload for the solar field and the generation of more solar thermal energy output. The sensitivity assessment results for the effect of solar multiple are summarized in Figure 10. With increasing the solar multiple from 1 to 3, the total annual solar field thermal energy output from the designed solar field is nearly doubled. The rate of the increase is more significant for the solar multiple values smaller than 2, compared to the values larger than 2. When the solar multiple increases from 2.2 to 3, the total solar thermal energy produced by the solar system increase from 126 to 137.4 GWh. Meanwhile, with the increase in the solar multiple from 1 to 1.4, the LCOE decreases significantly. However, the rate of decrement decreases upon the further increase in the solar multiple, reaching its

minimum at a solar multiple of 2. The reason is that the increase in capital cost for a larger plant overweighs the solar energy produced after the solar multiple values of two. Hence the solar multiple of two is the optimum value for the designed solar system.

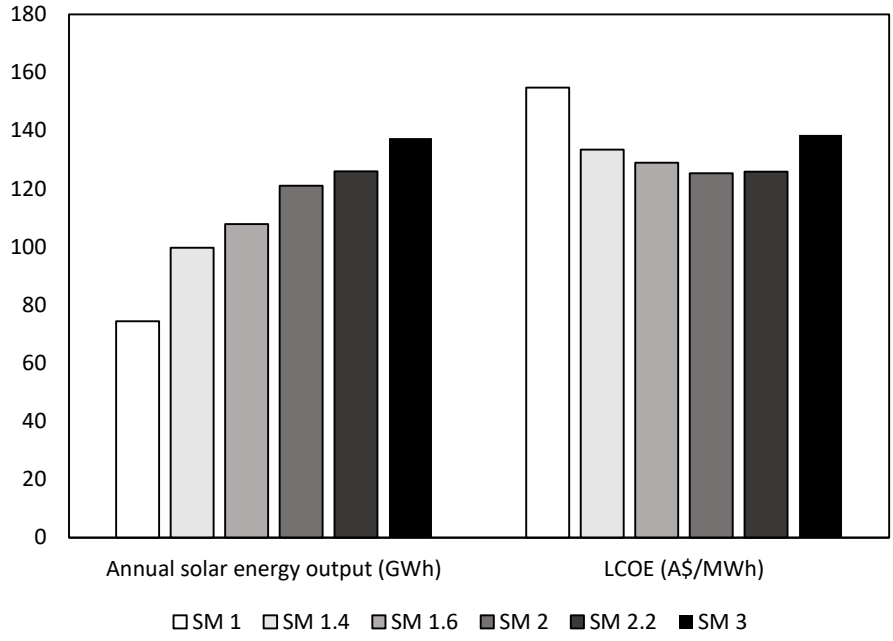

Figure 10 The effect of a change in the solar multiple (SM) on the annual solar thermal energy output and also LCOE for scenario 4

3.4.3 Effect of thermal energy storage duration

The TES is a way to store solar energy in a liquid medium to be used during the periods of no or low sunlight [62, 63]. The number of hours of storage duration is thus an important parameter affecting the volume of the storage tank and its TES capacity [64]. For a sensitivity analysis purpose, the TES period was changed from 1 hour in the base case to 10 h of storage. The sensitivity assessment results are presented in Figure 11. As can be seen, the annual solar field thermal energy output increases from 121 to 150 GWh upon a rise in the TES duration from 1 h to 6 h. Upon a further increase to 8 h, the amount of total thermal energy output is only increased slightly to 154.5 GWh. Meanwhile, the LCOE decreases from A$125.3/MWh

to A$103/MWh. Both the LCOE and the total thermal energy produced remain constant upon the further increase in the storage duration. An 8 h - long storage is optimum for the designed system.

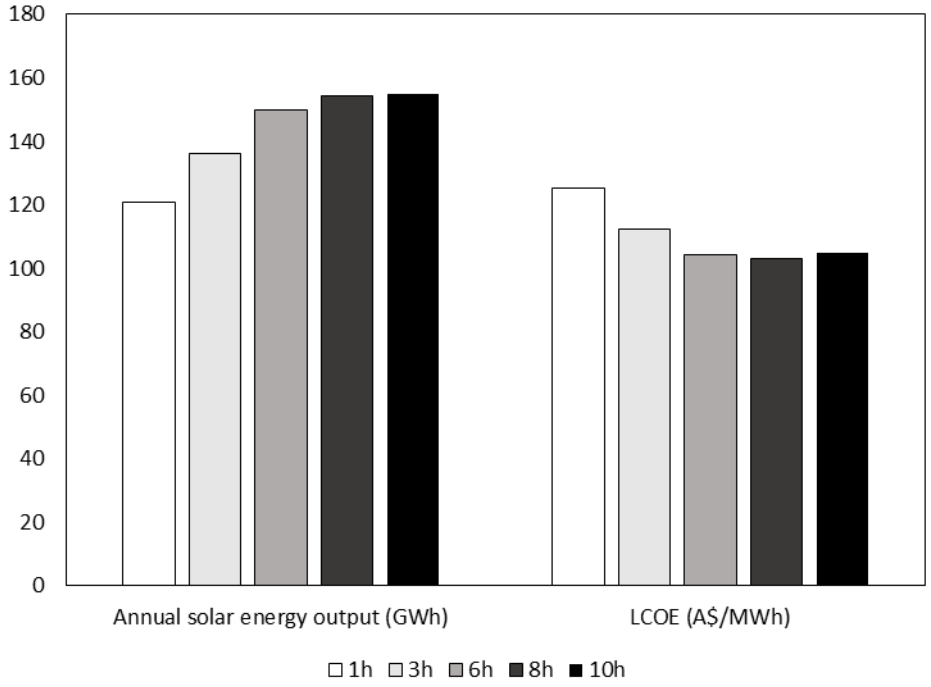

Figure 11 The effect of thermal energy hours of storage on the annual solar thermal energy output and also LCOE for scenario 4

3.5 The cost of the overall solar-assisted pyrolysis process

From the above sensitivity analyses, the design point D_{NI} of 750 W/m^2, a solar multiple of 2 and the energy storage of 8 h can be concluded as the optimized design parameters for scenario 4. Based on these optimum values, the preliminary capital and operating costs for scenarios 4 and scenario 1 are further calculated and presented in Table 5 and Table 6, respectively. The capital cost is the summation of all the purchased costs from the pyrolysis unit and the solar field. The results show a total investment of $113.4 million for a pyrolysis plant utilising 70.6 t/h of wet coal in the case of using solar thermal for both dryer and the pyrolysis reactor in scenario 4. Such a cost is almost three times more expensive than the

reference pyrolysis plant where the total capital cost is only $41 million [38]. For scenario 1 utilising the CSP for the dryer only, the capital cost from the pyrolysis equipment increases slightly from $34.6 million in the case of scenario 4 to $37.45 million, due to the requirement of extra combustor and compressor for the burning of coal gas. However, the overall capital cost for scenario 1 is much lower than in scenario 4. The use of PTC in scenario 1 is another reason for this. As can be noted from Table 6, scenario 4 has a higher operating cost ($27.33 million) compared to scenario 1 ($21.07 million). The major reason is that a huge amount of natural gas has to be purchased to supplement the solar thermal to accommodate the high energy demand. However, the net amount of products left for selling in scenario 4 is more than scenario 1 since no coal gas is burnt for heat provision. Total fixed charges, depreciation and capital were calculated as a percentage of the total capital cost. These assumptions led to a total production cost of $24.44 million for the pyrolysis sub-section and $2.89 million for the solar system sub-section for scenario 4. For scenario 1, the total fixed charges and depreciation & capital for the pyrolysis sub-section are more than scenario 4, since the capital cost for this subsection is larger. The total operating cost of the solar subsection for scenario 1 is $0.3 million which is much lower than that of scenario 4 with $2.89 million. The reason is the lower operating cost of a PTC compared to a ST which needed a bigger solar field, land and more water for maintenance.

Efforts were also made to compare the designed system with other solar power hybridized systems from the process techno-economic analysis perspective. So far, only a few studies on gasification of different carbonaceous materials have been found [65]. Saw at el. carried out a techno-economic analysis for a solar hybridized coal-to-liquid plant via gasification in Australia. They reported a much higher total capital cost of $493 million for a coal flow rate of 31.2 t/h (db), relative to 24.7 t/h (db) coal inlet flow rate in this study. The major reason is

175 the high cost of equipment, especially the gasifier and complexity of their process. They also
176 reported a capital cost of $377 million for the conventional coal-to-liquid plant with the use
177 of an entrained flow gasifier contributing to 18% of the total capital cost. Air separation unit
178 is another expensive unit comprising 16% of the total capital cost. In addition to these capital-
179 intensive units, there are two turbines (steam turbine and gas turbine), CO_2 compression unit
180 and a couple of refining and cleaning steps. These extra units make the coal-to-liquid-
181 process very complex and not comparable with the current process [36].

182

183 Finally, the capital cost and operating cost of the plant for both scenarios 1 and 4 was used as
184 an input for NPV analysis. The details of the NPV analysis and the assumptions used in this
185 calculation is described in our previous work [38]. The results are presented in Table 7. The
186 solar-assisted pyrolysis in scenario 1 is the most profitable option with a high NPV of $81.1
187 million and a short payback period of 4.85 years. Replacing the dryer heat supply with a
188 medium-temperature solar thermal seems attractive from both the economic and
189 environmental perspective. Conversely, scenario 4 cannot compete against the conventional
190 pyrolysis process, due to its considerably low NPV value of only $4.51 million and a
191 relatively long payback period of 12.3 years.

192

193 **Table 5** Capital cost and its breakdown for Scenario 1 and optimized Scenario 4

Capital cost items	Basis	Scenario 4	Scenario 1	Note
		Cost ($M ex. GST)		
Direct Plant Costs				
Equipment Purchase	EPC[a]	7.30	7.90	From APEA
Freight	10 % of EPC	0.73	0.79	
Direct equipment cost (DEC)	EPC + Freight	8.03	8.69	From CSIRO Cost calculation
Installation	45 % of DEC[b]	3.61	3.91	
Instrumentation	25 % of DEC	2.01	2.17	
Minor piping	16 % of EPC	1.17	1.26	

Structural	15% of EPC	1.10	1.19	
Electrical	25 % of DEC	2.01	2.17	
Buildings	25 % of EPC	1.83	1.98	
Yard Improvements	15 % of EPC	1.10	1.19	
Service Facilities	40 % of EPC	2.92	3.16	
HSE Functions	10 % of EPC	0.73	0.79	
Total Indirect Costs				
Engineering Supervision	50 % of DEC	4.02	4.35	
Legal Expenses	4 % of DEC	0.32	0.35	
Construction Expenses	40 % of DEC	3.21	3.48	
Working Capital				
Working Capital	8% of Direct plant cost + Total indirect costs	2.56	2.77	
Total Capital (pyrolysis)		34.60	37.45	
Total Capital (Solar)		78.80	18.37	From SAM
Total Capital cost		113.40	55.82	

194

195 **Table 6** Operating cost and its breakdown for Scenario 1 and optimized Scenario 4

Item	Scenario 4	Scenario 1	Assumptions	Price per unit
	Total cost ($M)			
Raw Materials				
Coal	1.98	1.98		$3.5/t
Sulfuric acid (98%)	0.002	0.002		$313/t
Ethanol	0.46	0.46	565 (t/a)	$813/t
Utilities				
Electricity	2.17	2.17		$0.1/ kWh
Natural Gas	8.37	4.57		$5 /GJ
Cooling water	0.11	0.11		$0.76/MWh
Air	0	0		Free
Total fixed charges			Assumptions	Price per unit
Labour	4.79	4.37		$25/t product
Maintenance and repairs	1.73	1.87	5% of total capital cost	NA
Operating supplies	0.35	0.37	1% of total capital cost	NA
Taxes (property)	0.69	0.75	2% of total capital cost	NA
Insurance	0.35	0.37	1% of total capital cost	NA
Depreciation & Capital				
Fixed Capital Depreciation	1.73	1.87	5% of total capital cost	NA
Interest on capital	1.73	1.87	5% of total capital cost	NA
Total Product Cost (pyrolysis)	24.44	20.77		
Total Product Cost (solar)	2.89	0.3		
Total Product Cost	27.33	21.07		

196 **Table 7** Comparison of NPV analysis for conventional pyrolysis and solar assisted scenarios
197 4 and 1

	Conventional pyrolysis [38]	Solar assisted pyrolysis (Scenario 4)	Solar assisted pyrolysis (Scenario 1)
Net present value (NPV) $M	52.8	4.51	81.1
Internal rate of return (IRR) %	25	9.5	26.7
Payback period (Year)	5.1	12.3	4.85

198

199 **4. Conclusions and Future Directions**

200 This paper examined the technical and economic feasibility of the integration of CSP into
201 Victorian brown coal utilization via a drying-pyrolysis process. Three different tools were
202 coupled to design the process and to assess the viability of four different design scenarios.
203 The most comprehensive scenario was further optimized through sensitivity analyses. The
204 major conclusions can be drawn as follows:

205 1) The plant operation analysis showed that integrating CSP with the pyrolysis process
206 can provide an average of 12.82% of the annual energy demands of the process in the
207 most comprehensive scenario 4 using ST to provide heat for both coal drying and
208 pyrolysis. The pyrolysis gas yield is the highest in scenario 4, reaching 10 t/h since
209 there is no need to burn the pyrolysis gas for energy provision purposes.
210 2) For the best ST design to be integrated into the pyrolysis process, a solar salt with a
211 solar multiple of 2, using carbonate salts as HTF, a design point D_{NI} of 750 W/m^2 and
212 the heat storage capacity of 8h shows a better performance in terms of the total solar
213 energy output over a year and also the LCOE.
214 3) From the economical perspective, the PTC system designed to cover the heat required
215 for the dryer only is economically viable. It even shows a slightly better economic
216 performance compared to the conventional pyrolysis process. The PTC system
217 assisted pyrolysis process has the potential to reach a high NPV value of $81.1

million and a short payback period of 4.85 years, relative to an NPV of $52.8 million and a payback period of 5.1 years for the conventional pyrolysis process. The use of ST for both drying and high-temperature pyrolysis is economically infeasible because of the high cost of the CSP component.

4) Hybridization of CSP with the other energy technologies for the production of solar fuels could potentially provide a lower risk and faster route to market rather than stand-alone systems. In addition to implementing government incentives, extensive research is needed in this area to decrease the cost of the CSP plants. Such cost reductions are expected to result from technical improvements, improvement in the efficiency of energy conversion, reduction in operation and maintenance cost and faster and more efficienct on-site construction. Development of advanced high temperature TES systems and larger linear collectors have been the major focuses of the international researchers in CSP cost reduction [66].

Acknowledgement

The authors gratefully acknowledge the financial support for this work by Coal Energy Australia Limited (CEA), ARC Industrial Research Training Hub (15010006) and ARC Linkage Project (LP160101228).

Declaration of interest

There is no conflict of interest to declare

References

[1] W. Liu, D. King, J. Liu, B. Johnson, Y. Wang, Z. Yang, Critical material and process issues for CO 2 separation from coal-powered plants, Jom, 61 (2009) 36-44.
[2] S. Schröders, H.-J. Allelein, Energy economic evaluation of process heat supply by solar tower and high temperature reactor based on the ammonia production process, Applied energy, 212 (2018) 622-639.
[3] G.J. Nathan, M. Jafarian, B.B. Dally, W.L. Saw, P.J. Ashman, E. Hu, A. Steinfeld, Solar thermal hybrids for combustion power plant: A growing opportunity, Progress in Energy and Combustion Science, 64 (2018) 4-28.
[4] Renewables 2019, IEA, Paris, 2019.
[5] K. Onarheim, Y. Solantausta, J. Lehto, Process Simulation Development of Fast Pyrolysis of Wood Using Aspen Plus, Energy & Fuels, 29 (2015) 205-217.
[6] Y. Qi, W. Hann, D.J.N. Subagyono, Y. Fei, M. Marshall, W.R. Jackson, A.F. Patti, A.L. Chaffee, Characterisation of the products of low temperature pyrolysis of Victorian brown coal in a semi-continuous/flow through system, Fuel, 234 (2018) 1422-1430.
[7] H. Weldekidan, V. Strezov, G. Town, Review of solar energy for biofuel extraction, Renewable and Sustainable Energy Reviews, 88 (2018) 184-192.
[8] J. Ward, M.G. Rasul, M.M.K. Bhuiya, Energy Recovery from Biomass by Fast Pyrolysis, Procedia Engineering, 90 (2014) 669-674.
[9] K. Zeng, G. Flamant, D. Gauthier, E. Guillot, Solar Pyrolysis of Wood in a Lab-scale Solar Reactor: Influence of Temperature and Sweep Gas Flow Rate on Products Distribution, Energy Procedia, 69 (2015) 1849-1858.
[10] X. Li, Y. Shen, X. Kan, T.K. Hardiman, Y. Dai, C.-H. Wang, Thermodynamic assessment of a solar/autothermal hybrid gasification CCHP system with an indirectly radiative reactor, Energy, 142 (2018) 201-214.
[11] M. Rahman, M. Aziz, Solar pyrolysis of scrap tire: optimization of operating parameters, Journal of Material Cycles and Waste Management, (2017) 1-9.
[12] A. Chinnici, G.J. Nathan, B.B. Dally, An experimental study of the stability and performance characteristics of a Hybrid Solar Receiver Combustor operated in the MILD combustion regime, Proceedings of the Combustion Institute, 37 (2019) 5687-5695.
[13] M.J. Antal, L. Hofmann, J. Moreira, C.T. Brown, R. Steenblik, Design and operation of a solar fired biomass flash pyrolysis reactor, Solar Energy, 30 (1983) 299-312.
[14] S. Morales, R. Miranda, D. Bustos, T. Cazares, H. Tran, Solar biomass pyrolysis for the production of bio-fuels and chemical commodities, Journal of Analytical and Applied Pyrolysis, 109 (2014) 65-78.
[15] R. Li, K. Zeng, J. Soria, G. Mazza, D. Gauthier, R. Rodriguez, G. Flamant, Product distribution from solar pyrolysis of agricultural and forestry biomass residues, Renewable Energy, 89 (2016) 27-35.
[16] J. Soria, K. Zeng, D. Asensio, D. Gauthier, G. Flamant, G. Mazza, Comprehensive CFD modelling of solar fast pyrolysis of beech wood pellets, Fuel Processing Technology, 158 (2017) 226-237.
[17] K. Zeng, D. Gauthier, D.P. Minh, E. Weiss-Hortala, A. Nzihou, G. Flamant, Characterization of solar fuels obtained from beech wood solar pyrolysis, Fuel, 188 (2017) 285-293.
[18] H. Wu, D. Gauthier, Y. Yu, X. Gao, G. Flamant, Solar-Thermal Pyrolysis of Mallee Wood at High Temperatures, Energy & Fuels, 32 (2018) 4350-4356.
[19] O. Authier, M. Ferrer, G. Mauviel, A.-E. Khalfi, J. Lede, Wood fast pyrolysis: comparison of Lagrangian and Eulerian modeling approaches with experimental measurements, Industrial & engineering chemistry research, 48 (2009) 4796-4809.
[20] M.U. Joardder, P. Halder, A. Rahim, N. Paul, Solar assisted fast pyrolysis: a novel approach of renewable energy production, Journal of engineering, 2014 (2014).
[21] G. Ramos, D. Pérez-Márquez, Design of semi-static solar concentrator for charcoal production, Energy Procedia, 57 (2014) 2167-2175.
[22] H. Grassmann, M. Boaro, Solar biomass pyrolysis with the linear mirror II, (2015).

[23] L. Arribas, N. Arconada, C. González-Fernández, C. Löhrl, J. González-Aguilar, M. Kaltschmitt, M. Romero, Solar-driven pyrolysis and gasification of low-grade carbonaceous materials, International journal of hydrogen energy, 42 (2017) 13598-13606.
[24] W.H. Beattie, R. Berjoan, J.-P. Coutures, High-temperature solar pyrolysis of coal, Solar Energy, 31 (1983) 137-143.
[25] J. Zeaiter, M.N. Ahmad, D. Rooney, B. Samneh, E. Shammas, Design of an automated solar concentrator for the pyrolysis of scrap rubber, Energy Conversion and Management, 101 (2015) 118-125.
[26] C. Ghenai, K. Alamara, A. Inayat, Solar Assisted Pyrolysis of Plastic Waste: Pyrolysis oil Characterization and Grid-Tied Solar PV Power System Design, Energy Procedia, 159 (2019) 123-129.
[27] V. Chintala, Production, upgradation and utilization of solar assisted pyrolysis fuels from biomass – A technical review, Renewable and Sustainable Energy Reviews, 90 (2018) 120-130.
[28] M. Sánchez, B. Clifford, J.D. Nixon, Modelling and evaluating a solar pyrolysis system, Renewable Energy, 116 (2018) 630-638.
[29] P. Guo, P.J. Van Eyk, W.L. Saw, P.J. Ashman, G.J. Nathan, E.B. Stechel, Performance assessment of Fischer–Tropsch liquid fuels production by solar hybridized dual fluidized bed gasification of lignite, Energy & Fuels, 29 (2015) 2738-2751.
[30] B.J. Hathaway, D.B. Kittelson, J.H. Davidson, Integration of solar gasification with conventional fuel production: the roles of storage and hybridization, Journal of solar energy engineering, 136 (2014).
[31] J. Suh, Y. Choi, Methods for converting monthly total irradiance data into hourly data to estimate electric power production from photovoltaic systems: A comparative study, Sustainability, 9 (2017) 1234.
[32] L. Guzman, A. Henao, R. Vasquez, Simulation and optimization of a parabolic trough solar power plant in the city of Barranquilla by using system advisor model (SAM), Energy Procedia, 57 (2014) 497-506.
[33] E.J. Sheu, A. Mitsos, A.A. Eter, E. Mokheimer, M.A. Habib, A. Al-Qutub, A review of hybrid solar–fossil fuel power generation systems and performance metrics, Journal of solar energy engineering, 134 (2012).
[34] M. Sudiro, A. Bertucco, Synthetic fuels by a limited CO2 emission process which uses both fossil and solar energy, Energy & fuels, 21 (2007) 3668-3675.
[35] A.A. Kaniyal, P.J. van Eyk, G.J. Nathan, P.J. Ashman, J.J. Pincus, Polygeneration of liquid fuels and electricity by the atmospheric pressure hybrid solar gasification of coal, Energy & Fuels, 27 (2013) 3538-3555.
[36] W. Saw, A. Kaniyal, P. van Eyk, G. Nathan, P. Ashman, Solar hybridized coal-to-liquids via gasification in Australia: techno-economic assessment, Energy Procedia, 69 (2015) 1819-1827.
[37] J. Zeaiter, F. Azizi, M. Lameh, D. Milani, H.Y. Ismail, A. Abbas, Waste tire pyrolysis using thermal solar energy: An integrated approach, Renewable Energy, 123 (2018) 44-51.
[38] T. Hosseini, A. De Girolamo, L. Zhang, Energy Evaluation and Techno-economic Analysis of Low-Rank Coal (Victorian Brown Coal) Utilization for the Production of Multi-products in a Drying–Pyrolysis Process, Energy & Fuels, (2018).
[39] K. Zeng, D. Gauthier, J. Soria, G. Mazza, G. Flamant, Solar pyrolysis of carbonaceous feedstocks: A review, Solar Energy, 156 (2017) 73-92.
[40] Solar Energy in: A.R.E. Agency (Ed.), 2018.
[41] Australian Energy Resources Assessment Australian Government 2013.
[42] T. Hosseini, C. Selomulya, N. Haque, L. Zhang, Indirect carbonation of Victorian brown coal fly ash for CO2 sequestration: Multiple-cycle leaching-carbonation and magnesium leaching kinetic modeling, Energy & Fuels, 28 (2014) 6481-6493.
[43] P. Denholm, M. Hummon, Simulating the value of concentrating solar power with thermal energy storage in a production cost model.
[44] T. Bouhal, Y. Agrouaz, T. Kousksou, A. Allouhi, T. El Rhafiki, A. Jamil, M. Bakkas, Technical feasibility of a sustainable Concentrated Solar Power in Morocco through an energy analysis, Renewable and Sustainable Energy Reviews, 81 (2018) 1087-1095.

[45] Y. Tian, C.-Y. Zhao, A review of solar collectors and thermal energy storage in solar thermal applications, Applied energy, 104 (2013) 538-553.
[46] M. Roeb, M. Neises, N. Monnerie, C. Sattler, R. Pitz-Paal, Technologies and trends in solar power and fuels, Energy & Environmental Science, 4 (2011) 2503-2511.
[47] R. Praveen, M.A. Baseer, A.B. Awan, M. Zubair, Performance Analysis and Optimization of a Parabolic Trough Solar Power Plant in the Middle East Region, Energies, 11 (2018) 1-18.
[48] R.G. Reddy, Novel molten salts thermal energy storage for concentrating solar power generation, Univ. of Alabama, Tuscaloosa, AL (United States), 2013.
[49] I.M. Serrano R., Concentrating Solar Thermal Technologies

Analysis and Optimisation by CFD Modelling, Springer 2017.
[50] A. Nzihou, G. Flamant, B. Stanmore, Synthetic fuels from biomass using concentrated solar energy–a review, Energy, 42 (2012) 121-131.
[51] A. Gil, M. Medrano, I. Martorell, A. Lázaro, P. Dolado, B. Zalba, L.F. Cabeza, State of the art on high temperature thermal energy storage for power generation. Part 1—Concepts, materials and modellization, Renewable and Sustainable Energy Reviews, 14 (2010) 31-55.
[52] P. Blanc, B. Espinar, N. Geuder, C. Gueymard, R. Meyer, R. Pitz-Paal, B. Reinhardt, D. Renné, M. Sengupta, L. Wald, S. Wilbert, Direct normal irradiance related definitions and applications: The circumsolar issue, Solar Energy, 110 (2014) 561-577.
[53] N.R.E.L. (NREL), SAM Advisor Model Help 2017.
[54] I.R.E.A. (IRENA), Concentrating Solar Power Power sector, 2012.
[55] S.F. Muradov N, Huang C, T-Raissi A, Decentralized production of hydrogen from hydrocarbons with reduced CO 2 emission, WHEC, Lyon France, 2006-June.
[56] N. Haque, W. Bruckard, J. Cuevas, A techno-economic comparison of pyrometallurgical and hydrometallurgical options for treating high-arsenic copper concentrates, XXVI International Mineral Processing Congress, New Delhi, India, 2012.
[57] T. Hosseini, N. Haque, C. Selomulya, L. Zhang, Mineral carbonation of Victorian brown coal fly ash using regenerative ammonium chloride – Process simulation and techno-economic analysis, Applied energy, 175 (2016) 54-68.
[58] A. De Girolamo, V. Tan, Z. Liu, L. Zhang, Pyrolysis of a lignite briquette – Experimental investigation and 1-dimensional modelling approach, Fuel, 212 (2018) 533-545.
[59] M. Alguacil, C. Prieto, A. Rodriguez, J. Lohr, Direct Steam Generation in Parabolic Trough Collectors, Energy Procedia, 49 (2014) 21-29.
[60] M. Seitz, S. Hübner, M. Johnson, Detailed partial load investigation of a thermal energy storage concept for solar thermal power plants with direct steam generation, AIP Conference Proceedings, AIP Publishing, 2016, pp. 050042.
[61] LAZARD, Lazard's levelized cost of energy analysis 2017.
[62] B.-c. Zhao, M.-s. Cheng, C. Liu, Z.-m. Dai, System-level performance optimization of molten-salt packed-bed thermal energy storage for concentrating solar power, Applied energy, 226 (2018) 225-239.
[63] Y. Tian, C.Y. Zhao, A review of solar collectors and thermal energy storage in solar thermal applications, Applied energy, 104 (2013) 538-553.
[64] I. Ortega-Fernández, I. Loroño, A. Faik, I. Uriz, J. Rodríguez-Aseguinolaza, B. D'Aguanno, Parametric analysis of a packed bed thermal energy storage system, AIP Conference Proceedings, AIP Publishing, 2017, pp. 080021.
[65] M. Pearce, M. Shemfe, C. Sansom, Techno-economic analysis of solar integrated hydrothermal liquefaction of microalgae, Applied energy, 166 (2016) 19-26.
[66] I.T.P. Limited, Concentrating Solar Thermal Technology Status - Informing a CSP Roadmap for Australia, in: A.R.E.A. (ARENA) (Ed.), 2018.